HNUE JOURNAL OF SCIENCE
Natural Science, 2025, Volume 70, Issue 1, pp. 25-35
This paper is available online at http://hnuejs.edu.vn/ns
DOI: 10.18173/2354-1059.2025-0004

PHENOMENOLOGICAL ANALOGY BETWEEN GROSS–PITAEVSKII THEORY FOR BOSE–EINSTEIN CONDENSATE MIXTURES IN INFINITE SPACE AND CLASSICAL MECHANICS

Pham Duy Thanh[1,*], Tran Ky Vi[2] and Nguyen Van Thu[1]
[1]*Faculty of Physics, Hanoi Pedagogical University 2, Vinh Phuc province, Vietnam*
[2]*Faculty of Semiconductor Technology, Dai Nam University, Hanoi city, Vietnam*
*Corresponding author: Pham Duy Thanh, e-mail: thanhdpham@outlook.com

Received February 04, 2025. Revised February 28, 2025. Accepted March 31, 2025.

Abstract. Based on an analogy between the Gross-Pitaevskii (GP) equations for binary mixtures of Bose-Einstein condensates (BECs) at zero temperature and Newton's equations of motion for a particle in a conservative field, we derive exact analytical solutions for the coupled GP equations in several phase-segregated BEC scenarios. In a straightforward manner, exact analytical solutions are obtained for both the symmetric and anti-symmetric cases. Furthermore, our approach enables us to propose approximate analytical solutions as an alternative to those derived from the widely used double-parabola approximation (DPA). Numerical computations demonstrate that our approximate solutions closely match the exact solutions within the GP framework. This finding is of particular significance for determining the wavefunctions of the condensates, a fundamental task in investigating the static properties of BECs.
Keywords: Bose-Einstein condensate, Gross-Pitaevskii equations, Newton's equation of motion, Phenomenological analogy.

1. Introduction

As is well known, a system of Bose gas undergoes a phase transition from a non-condensed phase to a condensed phase when it is cooled to a critical temperature [1], [2]. As the gas is cooled further below the critical temperature, a large fraction of the bosonic atoms rapidly falls into the ground state, a phenomenon known as Bose–Einstein condensation. The first "pure" BEC was created by Eric Cornell, Carl Wieman, et al. at JILA in June 1995, by cooling a dilute vapor of approximately two thousand rubidium-87 atoms to below 170 nK [3]. Theoretically, at zero temperature, all atoms are in the ground state [4]. In this case, the state of the system is described by a wavefunction that obeys the GP equation.

In the case of two-component BECs, the ground state is characterized by wavefunctions that satisfy the coupled GP equations [5]. These equations, which take the form of coupled differential equations, are considered nonlinear Schrödinger equations. Once the coupled GP equations are solved, all static and dynamic properties of the system can be analyzed. Considerable attention has been devoted to finding analytical solutions to these equations. However, it has been shown that analytical solutions are attainable only in certain special cases, while in most other instances, numerical methods must be used.

In Ref. [6], in the physical context of domain boundaries in convection patterns, Malomed et al. derived analytical solutions to the coupled GP equations under a symmetric condition, where the interspecies interaction was assigned a specific value, and the healing lengths of the two components were assumed identical. By decoupling the GP equations through the linearization of wavefunctions around their bulk values, Ao and Chui (1998) [7] obtained analytical solutions for the wavefunctions of each domain. A notable effort to analytically solve the coupled GP equations for all phase-segregated cases was made by Joseph et al. in Ref. [8] through the so-called double–parabola approximation (DPA). In this approach, the quartic order of the GP potential is approximated by two quadratic orders. As an alternative, this study focuses on exploring the phenomenological analogy between GP theory and Newtonian mechanics to derive analytical solutions for the coupled GP equations in several cases. Although this approach is not new, it has never been applied to solve the coupled GP equations.

2. Content

2.1. Gross–Pitaevskii theoretical framework

We start from the Lagrangian density of a BEC in the absence of an external field, within the mean–field GP theory [5]

$$\mathcal{L}\left(\Psi_1,\Psi_2\right)=\sum_{j=1}^{2}\left\{\frac{i\hbar}{2}\left(\Psi_j^*\frac{\partial\Psi_j}{\partial t}-\Psi_j\frac{\partial\Psi_j^*}{\partial t}\right)-\frac{\hbar^2}{2m_j}|\nabla\Psi_j|^2-\frac{g_{jj}}{2}|\Psi_j|^4-g_{12}|\Psi_1|^2|\Psi_2|^2\right\}, \tag{2.1}$$

where $\Psi_j=\Psi_j(\mathbf{r},t)$ is the wavefunction of component j $(j=1,2)$, depending on both coordinate $\mathbf{r}_j$ and time t; m_j is the atomic mass. For dilute, weakly interacting Bose gases, we only consider pairwise interactions; the simultaneous interaction among three or more particles can be neglected. Accordingly, the strength of the repulsive interaction between two particles is characterized by

$$g_{ij}=2\pi\hbar^2 a_{ij}\left(\frac{1}{m_i}+\frac{1}{m_j}\right)>0, \tag{2.2}$$

with a_{ij} being the s-wave scattering length in the Born approximation.

Next, we rewrite the Lagrangian density by applying a transformation

$$\Psi_j(\mathbf{r}_j,t)\equiv\Phi_j(\mathbf{r}_j,t)\exp\left(-i\frac{\mu_j t}{\hbar}\right), \tag{2.3}$$

where μ_j is the chemical potential of component j. By substituting (2.3) into (2.1), we obtain a Lagrangian density in terms of the new wavefunctions Φ_j:

$$\tilde{\mathcal{L}} = \sum_{j=1}^{2} \left\{ \Phi_j^* \left(i\hbar \frac{\partial}{\partial t} - \frac{\hbar^2}{2m_j} \nabla^2 \right) \Phi_j + \mu_j |\Phi_j|^2 - \frac{g_{jj}}{2} |\Phi_j|^4 \right\} - g_{12} |\Phi_1|^2 |\Phi_2|^2. \quad (2.4)$$

Substituting this Lagrangian density into the Euler–Lagrange (EL) equations,

$$\frac{\partial \tilde{\mathcal{L}}}{\partial \Phi_j^*} = \partial_t \frac{\partial \tilde{\mathcal{L}}}{\partial \left(\partial_t \Phi_j^* \right)}, \; j = 1, 2, \quad (2.5)$$

yields the time-dependent GP equations

$$i\hbar \frac{\partial \Phi_j}{\partial t} = -\frac{\hbar^2}{2m_j} \nabla^2 \Phi_j + \frac{\partial V_{\mathrm{GP}}}{\partial \Phi_j^*}, \quad (2.6)$$

where

$$V_{\mathrm{GP}} = \sum_{j=1}^{2} \left(-\mu_j |\Phi_{j0}|^2 + \frac{g_{jj}}{2} |\Phi_{j0}|^4 \right) + g_{12} |\Phi_{10}|^2 |\Phi_{20}|^2, \quad (2.7)$$

is known as the GP potential energy density. In the ground state, the wavefunction Φ_j is time-independent, i.e., $\Phi_j(\mathbf{r}, t) = \Phi_{j0}(\mathbf{r})$. Then Eqs. (2.6) become the time-independent GP equations

$$\frac{\hbar^2}{2m_j} \nabla^2 \Phi_{j0} = \frac{\partial V_{GP}}{\partial \Phi_{j0}^*}. \quad (2.8)$$

By substituting (2.7) into (2.8), we obtain a system of nonlinear differential equations for the wavefunctions

$$\left(-\frac{\hbar^2}{2m_j} \nabla^2 + g_{jj} |\Phi_{j0}|^2 + g_{12} |\Phi_{j'0}|^2 \right) \Phi_{j0} = \mu_j \Phi_{j0},$$
$$j = (1, 2), \; (j \neq j'). \quad (2.9)$$

To simplify notation, we use the following dimensionless quantities

$$\phi_j = \frac{\Phi_{j0}}{\sqrt{n_{j0}}}, \; K = \frac{g_{12}}{\sqrt{g_{11} g_{22}}} > 1, \; \tilde{\mathbf{r}}_j = \frac{\mathbf{r}_j}{\xi_1}, \quad (2.10)$$

where $\xi_j = \dfrac{\hbar}{\sqrt{2m_j \mu_j}}$ is the healing length, and $n_{j0} = \dfrac{\mu_j}{g_{jj}}$ is the number density of condensate j in bulk. In this study, we focus on the regime $K > 1$, corresponding to immiscible condensates [7]. The GP potential density and Eq. (2.9) reduce to the dimensionless form

$$\tilde{V}_{\mathrm{GP}} = \sum_{j=1}^{2} \left(-|\phi_j|^2 + \frac{|\phi_j|^4}{2} \right) + K |\phi_1|^2 |\phi_2|^2, \quad (2.11)$$

and

$$\left\{-\left(\frac{\xi_j}{\xi_1}\right)^2\frac{\partial^2}{\partial\tilde{\mathbf{r}}_j^2}+|\phi_j|^2+K|\phi_{j'}|^2\right\}\phi_j=\phi_j. \tag{2.12}$$

For describing a static planar interface at $z=0$, separating bulk condensate 1 in the half-space $z\geq 0$ and bulk condensate 2 in the half-space $z\leq 0$, we restrict our attention to wavefunctions that are translationally invariant in x and y. To keep notation simple, we do not change the function's name: $\phi_j(\tilde{\mathbf{r}}_j)\rightarrow\phi_j(\tilde{z})$. For describing an interface, the coupled dimensionless time-independent GP equations take the form

$$-\phi_j+\phi_j^3+K\phi_{j'}^2\phi_j=\left(\frac{\xi_j}{\xi_1}\right)^2\frac{d^2\phi_j}{d\tilde{z}^2}, \tag{2.13}$$

with the boundary conditions

$$\begin{aligned}\phi_1(-\infty)&=\phi_2(\infty)=0,\\ \phi_2(-\infty)&=\phi_1(\infty)=1.\end{aligned} \tag{2.14}$$

2.2. Exact analytical solutions

In this paper, we utilize the idea introduced by Van Schaeybroeck et al. (2022) [9] to explore the phenomenological analogy from a dynamical perspective. We consider Eqs. (2.13) as Newton's second-law equations for a particle, where the evolution in the spatial coordinate z is analogized to evolution in time. A particle of mass $m=2$ moves on the $(\phi_1,\xi\phi_2)$ plane, where $\xi=\xi_2/\xi_1$, and the force components are given by

$$\begin{aligned}F_1&=2\left(-\phi_1+\phi_1^3+K\phi_2^2\phi_1\right)=-\frac{\partial U}{\partial\phi_1},\\ F_2&=\frac{2}{\xi}\left(-\phi_2+\phi_2^3+K\phi_1^2\phi_2\right)=-\frac{\partial U}{\partial(\xi\phi_2)},\end{aligned} \tag{2.15}$$

where U is the potential energy of the particle. It is straightforward to see that

$$U=-\tilde{V}_{\mathrm{GP}}=\sum_{j=1}^{2}\left(\phi_j^2-\frac{\phi_j^4}{2}\right)-K\phi_1^2\phi_2^2. \tag{2.16}$$

The kinetic energy of the particle is

$$T=\left(\frac{d\phi_1}{d\tilde{z}}\right)^2+\left(\xi\frac{d\phi_2}{d\tilde{z}}\right)^2. \tag{2.17}$$

From classical mechanics, it is clear that the mechanical energy E of the particle is conserved

$$E=T+U=\left(\frac{d\phi_1}{d\tilde{z}}\right)^2+\left(\xi\frac{d\phi_2}{d\tilde{z}}\right)^2+\sum_{j=1}^{2}\left(\phi_j^2-\frac{\phi_j^4}{2}\right)-K\phi_1^2\phi_2^2=\frac{1}{2}. \tag{2.18}$$

The position (ϕ_{10}, ϕ_{20}) that corresponds to the minimum value $U_{\rm m}$ of the potential field is determined by the condition

$$F_1(\phi_{10}, \phi_{20}) = F_2(\phi_{10}, \phi_{20}) = 0. \tag{2.19}$$

Combining (2.15) and (2.19), we obtain

$$\phi_{10} = \phi_{20} = \frac{1}{\sqrt{1+K}}, \quad U_{\rm m} = \frac{1}{1+K}. \tag{2.20}$$

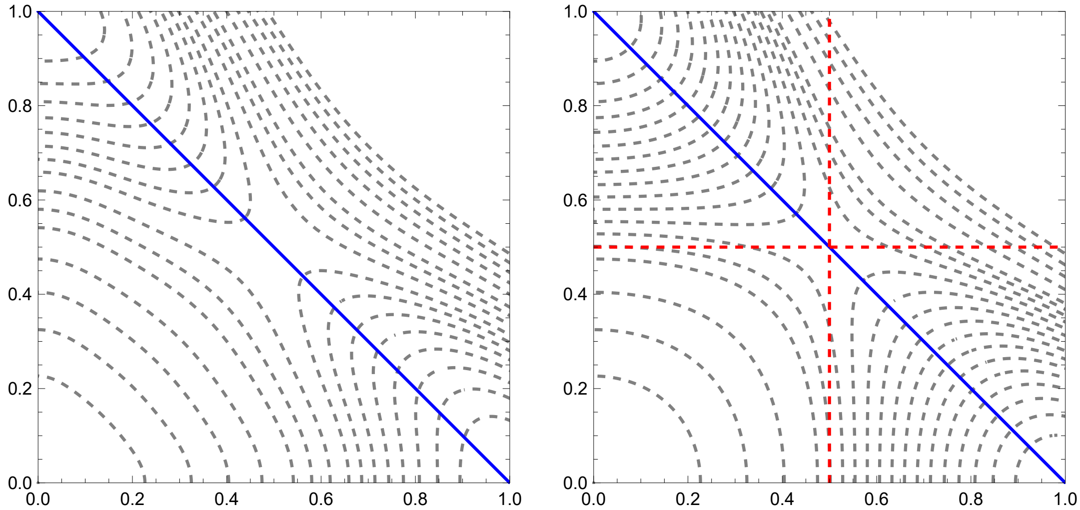

Figure 1. The dashed gray lines are the equipotential lines for $K = 2$ (left figure) and $K = 3$ (right figure). The solid blue line is the particle trajectory on the (ϕ_1, ϕ_2) coordinate plane for $\xi = 1$, $K = 3$. The intersection of the two dashed red lines is the point of lowest potential energy in the field

First, we consider the simplest case, $\xi = 1$: the particle moves along a straight line from $(0, 1)$ to $(1, 0)$ in the (ϕ_1, ϕ_2) coordinate plane (see Figure 1). In this case, the particle initially has no kinetic energy; it accelerates from $(0, 1)$ toward the position of lowest potential energy, $(1/2, 1/2)$. After passing this point, its kinetic energy gradually decreases to zero, and it stops at $(1, 0)$. From $\phi_{10} = \phi_{20} = 1/2$, it is easy to see that this case corresponds to $K = 3$. By substituting $K = 3$ into (2.18) and combining with the trajectory equation $\phi_2 = 1 - \phi_1$, we obtain the equation of one-dimensional motion in the form

$$\frac{1}{2}\left(\frac{d\phi_1}{d\tilde{z}}\right)^2 - \phi_1^2(1-\phi_1)^2 = 0. \tag{2.21}$$

This differential equation can be solved analytically by the method of variable separation and then integrating both sides with the "initial condition" $\phi_1(0) = 1/2$. Hence, we obtain the reduced wavefunctions $\phi_j(\tilde{z})$ in Eqs. (2.13) for $K = 3$ and $\xi = 1$ as follows:

$$\phi_1(\tilde{z}) = \frac{1}{1+e^{-\sqrt{2}\tilde{z}}}, \quad \phi_2(\tilde{z}) = \frac{1}{1+e^{\sqrt{2}\tilde{z}}}. \tag{2.22}$$

The solutions in (2.22) coincide with Malomed's analytical solutions for coupled differential equations describing domain boundaries in convection patterns [6], which are mathematically identical to Eqs. (2.13) for $K = 3$ and $\xi = 1$.

To depict the equipotential curves as shown in Figure 1, we use a polar coordinate system where the coordinates r and θ satisfy

$$\phi_1 = r\cos\theta, \quad \phi_2 = r\sin\theta. \tag{2.23}$$

By substituting (2.23) into (2.16), we obtain the equation describing the equipotential line U

$$r(\theta) = \left(\frac{1 \pm \sqrt{1 - 2U\left\{1 + \frac{K-1}{2}\sin^2(2\theta)\right\}}}{1 + \frac{K-1}{2}\sin^2(2\theta)} \right)^{1/2}. \tag{2.24}$$

From the equipotential lines in Figure 1(b), we see that for $K = 3$, there is a field line—a straight line—passing through $(0, 1)$ and $(1, 0)$ in the wavefunction space, perpendicular to the equipotential lines at the "top of the hill." Therefore, for $K = 3$ and $\xi = 1$ (where ϕ_1 and ϕ_2 are symmetric), the particle moves strictly along this field line with zero initial velocity. This does not occur in other cases because the field lines perpendicular to the equipotential lines at the "top of the hill" are curved (an example is shown in Figure 1(a)), so the particle trajectory will also be curved. Thus, $K = 3$ and $\xi = 1$ is the simplest case.

Interestingly, another case where we find an exact analytical solution is $K = 1.5$ and $\xi = 0.5$. Based on the shape of the equipotential lines in the $(\phi_1, \phi_2/2)$ coordinate plane and the point where the potential field reaches its minimum value $(U_{\mathrm{m}} = 0.4)$ (see Figure 2), we predict that the particle follows a parabolic trajectory described by $\phi_2 = 1 - \phi_1^2$. In this case, Eq. (2.18) can be transformed into

$$\left(\frac{d\phi_1}{d\tilde{z}}\right)^2 + \frac{\phi_1^2(1-\phi_1^2)^2}{2} = 0. \tag{2.25}$$

The analytical solution obtained by solving the similar one-dimensional motion equation (2.25) is

$$\phi_1 = \frac{1}{\sqrt{1 + A^{-2}e^{-\sqrt{2}\tilde{z}}}}, \quad \phi_2 = \frac{1}{1 + A^2 e^{\sqrt{2}\tilde{z}}}, \tag{2.26}$$

where $A = \sqrt{\frac{1}{2}\left(\sqrt{5}-1\right)} \approx 0.786$. This constant is determined from the condition $\phi_1(0) = \phi_2(0)$, assuming the interface is at $z = 0$.

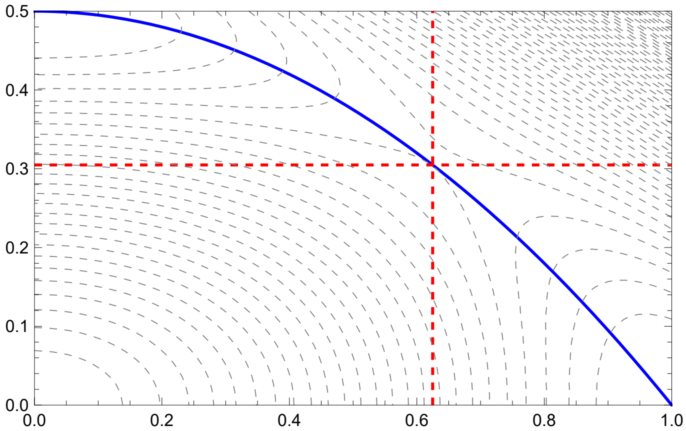

Figure 2. The particle trajectory (solid blue line) on the $(\phi_1, \phi_2/2)$ coordinate plane for $\xi = 0.5$ and $K = 1.5$, with equipotential curves in the background

Using the analytical results (2.22) and (2.26), we plot the reduced wavefunction of each component versus the dimensionless coordinate $\tilde{z} = z/\xi_1$ (see Figure 3). The graphs from the analytical results coincide with those obtained numerically.

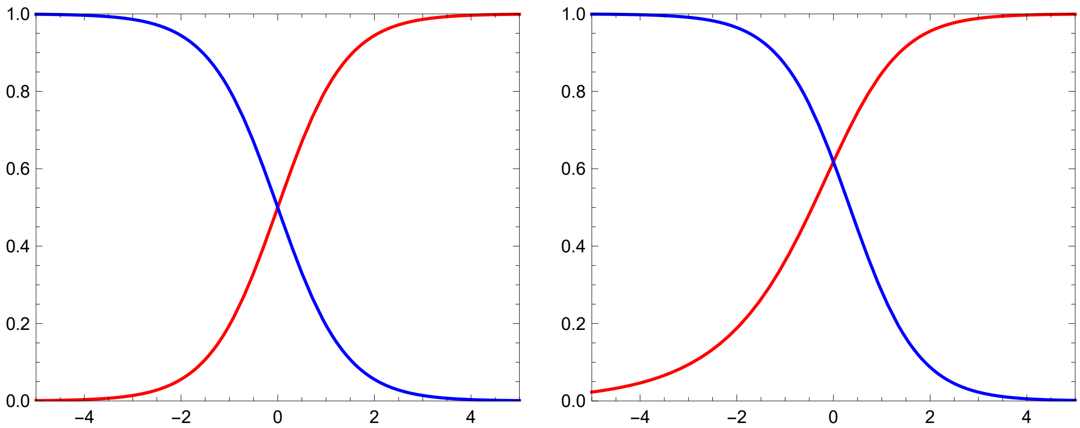

Figure 3. The reduced wavefunction profiles ϕ_1 (solid red line) and ϕ_2 (solid blue line), plotted versus $\tilde{z} = z/\xi_1$ for $\xi = 1$, $K = 3$ (left) and $\xi = 0.5$, $K = 1.5$ (right)

To conclude this section, we plot the kinetic and potential energies as functions of "time" $\tilde{z}$ to observe their variation. In Figure 4, we see that in both cases we examined, the particle's kinetic energy decreases from its maximum value to zero as $\tilde{z}$ increases from

0 to infinity. Meanwhile, the potential energy increases from its minimum value to its maximum value of $1/2$, which is also the particle's total mechanical energy. The dashed blue line represents the conservation of mechanical energy, consistent with Eq. (2.18).

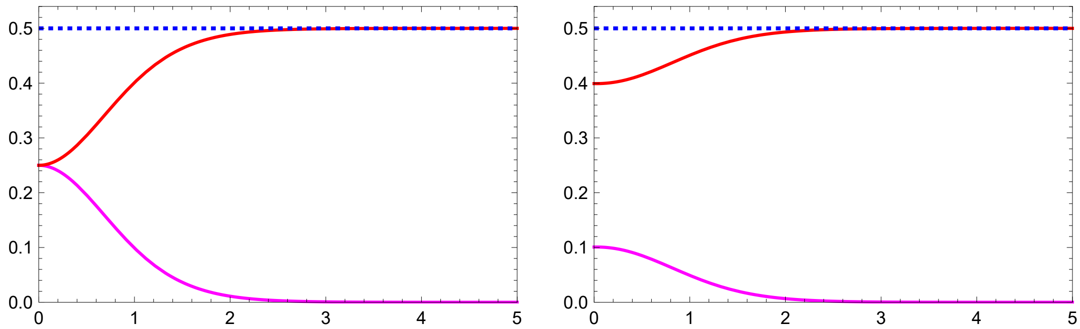

Figure 4. The potential energy U (solid red line), the kinetic energy (solid magenta line), and the total mechanical energy (dashed blue line), plotted versus $\tilde{z}$ for $\xi = 1$, $K = 3$ (left) and $\xi = 0.5$, $K = 1.5$ (right)

2.3. Approximate analytical solutions

The DPA for binary mixtures of BECs was introduced by Joseph O. Indekeu et al. in Ref. [8]. The main idea is to replace the GP potential with a harmonic potential (referred to as the DPA potential), so that the Euler–Lagrange equations reduce to two linear differential equations, allowing analytical solutions for the wavefunctions. Hauge was the first to employ this approximation to determine the surface free energy per unit area for systems with a two-component wavefunction within Landau theory [10]. Previous studies have shown that the profile plotted according to the DPA-based analytical expressions aligns well with the numerical solution [11]-[13]

We employ an expansion around the bulk condensate j, such that $j = 1$ and $j = 2$ for $z < 0$ and $z > 0$, respectively. This approach is elaborated below

$$\phi_j = a_j, \quad \phi_{j'} = 1 - b_{j'}, \tag{2.27}$$

where a_j and b_j are small real numbers. Substituting (2.27) into (2.11), we obtain the dimensionless potential energy density in the DPA model

$$\tilde{V}_{\mathrm{DPA}} = (K-1)\phi_j^2 + 2\left(\phi_{j'} - 1\right)^2 - \frac{1}{2}, \tag{2.28}$$

with $(j, j') = (1, 2)$ for $\tilde{z} \leq 0$ and $(j, j') = (2, 1)$ for $\tilde{z} \geq 0$. Substituting (2.28) into the time-independent GP equations (2.8) yields two linear differential equations, known as the double-parabola approximated GP equations

$$-\left(\frac{\xi_j}{\xi_1}\right)^2 \frac{d^2\phi_j}{d\tilde{z}^2} + (K-1)\phi_j = 0,$$
$$-\left(\frac{\xi_{j'}}{\xi_1}\right)^2 \frac{d^2\phi_{j'}}{d\tilde{z}^2} + 2(\phi_{j'}-1) = 0. \tag{2.29}$$

Combining the boundary conditions (2.14) and the continuity conditions for the order parameter and its first derivatives (equivalent to initial conditions), we obtain solutions of the form

$$\phi_j = \frac{\sqrt{2}}{\sqrt{2}+\sqrt{K-1}} \exp\left\{(-1)^{j+1}\frac{\xi_1\sqrt{K-1}}{\xi_j}\tilde{z}\right\},$$
$$\phi_{j'} = 1 - \frac{\sqrt{K-1}}{\sqrt{2}+\sqrt{K-1}} \exp\left\{(-1)^{j+1}\frac{\xi_1\sqrt{2}}{\xi_{j'}}\tilde{z}\right\}. \tag{2.30}$$

The advantage of DPA is that it can provide approximate solutions for all values of K and ξ. However, the wavefunction profiles in DPA can sometimes deviate noticeably from the numerical profiles. Motivated by the exact solutions (2.22) and (2.26) found in the previous section, we propose the following approximate solutions:

$$\phi_1(\tilde{z}) = \frac{1}{1+\exp\left(-\dfrac{2\tilde{z}}{\sqrt{1+\xi^2}}\right)},$$
$$\phi_2(\tilde{z}) = \frac{1}{1+\exp\left(\dfrac{2\tilde{z}}{\sqrt{1+\xi^2}}\right)}, \quad \text{for } K=3, \tag{2.31}$$

and

$$\phi_1(\tilde{z}) = \sqrt{1+\chi(\tilde{z})^2} - \chi(\tilde{z}),$$
$$\phi_2(\tilde{z}) = \frac{2\chi(\tilde{z})}{\chi(\tilde{z})+\sqrt{1+\chi(\tilde{z})^2}}, \quad \text{for } K=1.5, \tag{2.32}$$

where $\chi(\tilde{z}) = \dfrac{2e^{-\tilde{z}}}{1+4\xi^2}$.

In Figure 5, we compare our proposed reduced wavefunction profiles with the DPA model and the numerically exact solutions. These plots show that our proposed profiles match the numerically exact solutions more closely than the DPA model does. Furthermore, the values of the reduced wavefunctions at the interface are also indicated more accurately.

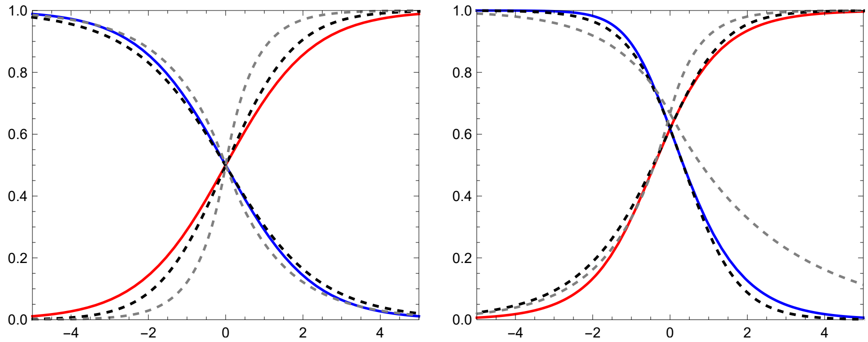

Figure 5. The reduced wavefunction profiles ϕ_1 and ϕ_2, plotted versus $\tilde{z} = z/\xi_1$ for $\xi = 2$, $K = 3$ (left) and $\xi = 2$, $K = 1.5$ (right). The proposed profiles (solid lines), the numerically exact profiles (dashed black lines), and the DPA profiles (dashed gray lines) are shown

3. Conclusions

In the foregoing sections, we presented the phenomenological analogy between the time-independent GP equation for binary BEC mixtures and Newton's second law of motion. In GP theory, the BEC state without an external field is fully described by its ground-state wavefunction, which is real and spatially dependent. Within this analogy, the wavefunction of each component (or the order parameter) acts like the coordinate of a non-relativistic particle moving in a two-dimensional potential field. Using this analogy, we showed exact solutions of the time-independent GP equation for a two-component BEC system in two cases: $K = 3$, $\xi_2/\xi_1 = 1$; and $K = 1.5$, $\xi_2/\xi_1 = 0.5$.

Additionally, we reviewed the DPA approximation for binary BEC mixtures, a method for finding approximate solutions to the time-independent GP equations. We compared the reduced order parameters from the DPA model with numerically exact profiles and with the profiles we proposed from the mechanical analogy, for $K = 3$ and $K = 1.5$. We found that the reduced wavefunction profiles corresponding to our proposed approximate solutions agree more closely with the numerically exact profiles than those derived from the DPA model.

Although this analogy is purely mathematical and based on observed phenomena, it provides valuable new insights into the solutions of coupled time-independent GP equations. We hope that the approach via the Newtonian analogy will be useful for both semi-finite and finite systems.

In the next research direction, analytical expressions for various static properties of two-component BEC mixtures (e.g., grand potential, interfacial tension) can be determined by employing the condensate wavefunctions presented in this paper. These analytical results may be closer to the numerical results than those obtained using the DPA model.

REFERENCES

[1] Bose SN, (1924). Plancks gesetz und lichtquantenhypothese. *Zeitschrift für Physik*, 26(1), 178–181.

[2] Einstein A, (1924). Quantentheorie des einatomigen idealen Gases. *Sitzungsberichte der Königlich Preussischen Akademie der Wissenschaften zu Berlin*, 22, 261–267.

[3] Anderson MH, Ensher JR, Matthews MR, Wieman CE & Cornell EA, (1995). Observation of Bose–Einstein condensation in a dilute atomic vapor. *Science*, 269(5221), 198–201.

[4] Pitaevskii L & Stringari S, (2003). *Bose–Einstein Condensation*. Oxford University Press, Oxford.

[5] Pethick CJ & Smith H, (2008). *Bose–Einstein condensation in dilute gases*. Cambridge University Press, Cambridge.

[6] Malomed BA, Nepomnyashchy AA & Tribelsky MI, (1990). Domain boundaries in convection patterns. *Physical Review A*, 42(12), 7244.

[7] Ao P & Chui ST, (1998). Binary Bose–Einstein condensate mixtures in weakly and strongly segregated phases. *Physical Review A*, 58(6), 4836.

[8] Indekeu JO, Lin CY, Nguyen VT, Van Schaeybroeck B & Tran HP, (2015). Static interfacial properties of Bose–Einstein–condensate mixtures. *Physical Review A*, 91(3), 033615.

[9] Van Schaeybroeck B, Navez P & Indekeu JO, (2022). Interface potential and line tension for Bose–Einstein condensate mixtures near a hard wall. *Physical Review A*, 105(5), 053309.

[10] Hauge EH, (1986). Landau theory of wetting in systems with a two-component order parameter. *Physical Review B*, 33(5), 3322.

[11] Nguyen VT, (2016). Static properties of Bose–Einstein condensate mixtures in semi-infinite space. *Physics Letters A*, 380(37), 2920–2924.

[12] Pham DT & Nguyen VT, (2024). Static Properties of Prewetting Phase in Binary Mixtures of Bose–Einstein Condensates. *International Journal of Theoretical Physics*, 63, 315.

[13] Tien LV, Huyen TTT, Huong VV, Bao CG, Hoc NQ, Vi TK, Dung LN, Lam LT, Hoa DT, Kien NT & Song PT, (2025). Interface's movement in the segregated binary mixture of two weakly interacting Bose–Einstein condensates. *Annals of Physics*, 475, 169947.